UNIVERSITY
OF APPLIED SCIENCES
UPPER AUSTRIA

Bachelor Major

Automation Engineering

HIGHSPEED SCHLIEREN PHOTOGRAPHY

submitted as Bachelor 1 thesis

to achieve the 5^{th} semester

Bachlor of Science

by

Marco Eder

January 2018

Thesis supervisors

FH-Prof. DI Dr. Peter Zeller

Prof. John Renie Ph.D.

UNIVERSITY OF APPLIED SCIENCES UPPER AUSTRIA

Sworn declaration

Wels Campus

I hereby declare that I prepared this work independently and without help from third parties, that I did not use sources other than the ones referenced and that I have indicated passages taken from those sources.

This thesis was not previously submitted in identical or similar form to any other examination board, nor was it published.

.....

Marco Eder
Wels, January 2018

Abstract

In general, the motion of electric arcs and how it is influenced among numerous parameter by the gas flow around the arc is not fully known. In order to investigate gaseous flows around an electric arc Schlieren Photography may be applied. This kind of photography, that in some cases requires additional optical equipment, in combination with image processing is able to not just make these flows visible but also to quantify them. It was the aim of the project to perform a feasibility study which kind of Schlieren Photography approach would be appropriate for high speed schlieren filming in the vicinity of an electric arc. The possible systems include dual-lens or dual-mirror systems and Background-oriented Schlieren [1]. All three of these systems have already been used for quantitative schlieren imaging before [2] [3]. For convenience only, no further equipment was bought for this research which is why the tests in this thesis are Background-oriented Schlieren only. A simple setup with a smartphone camera and projected and printed patterns was set up in order to test the post processing algorithms. The tests showed that the Background-oriented Schlieren setup was very sensitive to vibrations. Then again, Background-oriented Schlieren represents the cheapest possible schlieren setup. Based on the results of these tests and a literature research on dual-lens and dual-mirror schlieren systems, an appropriate schlieren system with respect to the intended application may be chosen.

Contents

1 Introduction

Whenever there is a fault in an electric circuit, the circuit must be interrupted as fast as possible in order to preserve the functionality of the components involved and the health in case of human involvement. This fast shut off is performed by a circuit breaker which disconnects the electrical system mechanically by opening a pair of contacts. The separation of the contact pair will induce an electric arc which must be extinguished as fast as possible in order to achieve a current limitation of the fault current [4]. Under certain circumstances such as high voltage, inductive loads that counteract the change of current or when interrupting DC systems at all, a stable arc may occur. This means, even though the circuit is no longer closed, the current keeps flowing via the conductive arc. A circuit breaker uses an arc chute to extinguish the arc in an effective manner. Thereby, how fast the short circuit can be interrupted is dependent on how fast the occurring arc can be driven into the arc chute. Driving the arc into the arc chute as quickly as possible is a complex process which can only be fully understood by knowing the gas dynamic boundary conditions influencing the arc motion. The gas dynamic processes may be observed by measuring parameters such as pressure, density and temperature. In order to obtain these physical quantities, Schlieren Photography may be applied. Schlieren Photography uses the deflection of light through transparent media caused by a change of the index of refraction [1]. This deflection may be interpreted with respect to spatial density, pressure and temperature distribution. Combined with high speed filming, fast gas flow phenomena such as pressure wave propagation or temperature distribution changes can be investigated.

2 Theory

2.1 Circuit Breakers and Arc Chutes

A circuit breaker is an essential safety component that can be found in every industrial plant or electrical system in order to protect human beings, machines and electrical components. Unlike a fuse, that must be replaced after a fault occurred in a system, a circuit breaker can be reset mechanically if the fault is fixed, otherwise it will interrupt the circuit again [4].

2.1.1 Operating Principle of Circuit Breakers

Whenever a fault occurs in an electrical system, the current increases significantly which can cause extensive damage to components or even failure. High fault current may damage the equipment due to thermal and mechanical overload. In order to prevent these kind of faults, a circuit breaker can be triggered in two different ways: by overcurrent which is triggered by a bimetal trigger and by a short circuit which is triggered by a magnetic trigger. Dependent on the value of the fault current the trigger will be faster with rising current values. The time-current behaviour is described by standardized trip curves [5].

Fig. 2.1 shows the principle design of a circuit breaker with the three most relevant arc extinguishing principles: arc elongation, arc cooling and arc splitting.

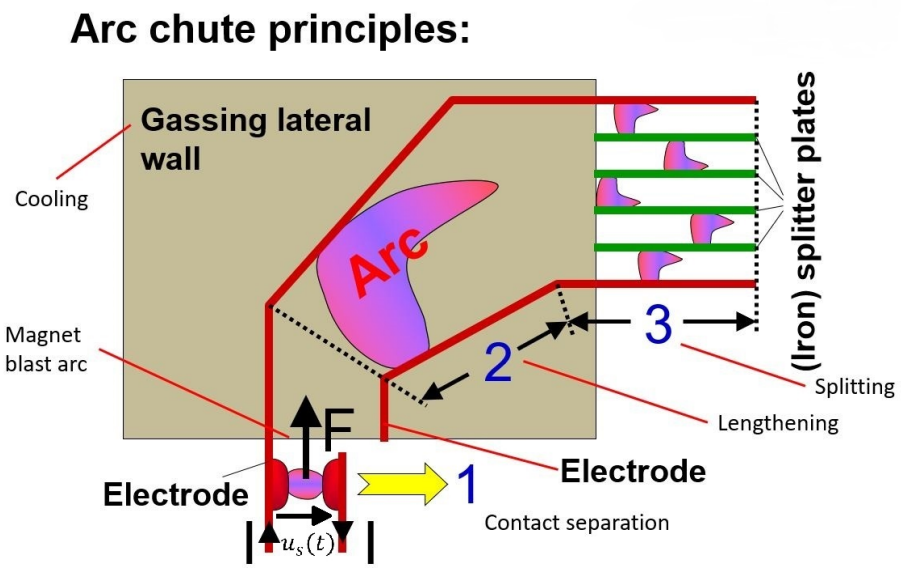

Fig. 2.1: Illustration of a circuit breaker with an electric arc that is being driven into the arc chute [6]

The equivalent circuit of a short circuit with consideration of the switching arc during a switching operation is shown in Fig. 2.2.

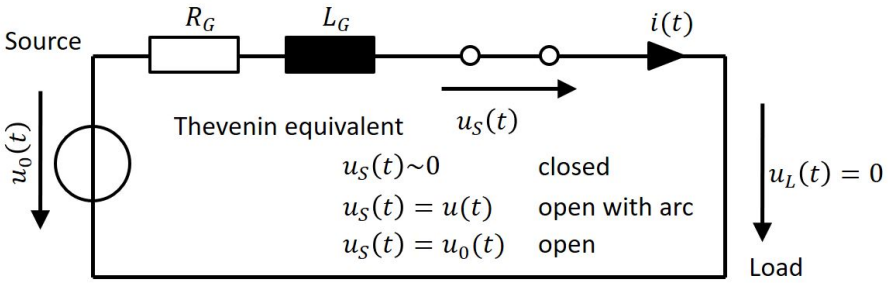

Fig. 2.2: Equivalent circuit of a switching operation with an arc occuring [6]

The differential equation that describes this circuit can be written as

$$i(t) \cdot R_G + \frac{di}{dt} \cdot L_G = u_0(t) - u_s(t). \qquad [2.1]$$

$i(t)$ represents the time-dependent current and $\frac{di}{dt}$ its derivative with respect to time, R_G and L_G represent the resistor and the inductance, respectively, $u_s(t)$ stands for the voltage across the switch and $u_0(t)$ stands for the source voltage. The voltage and current over time of a short circuit fault is shown in Fig. 2.3.

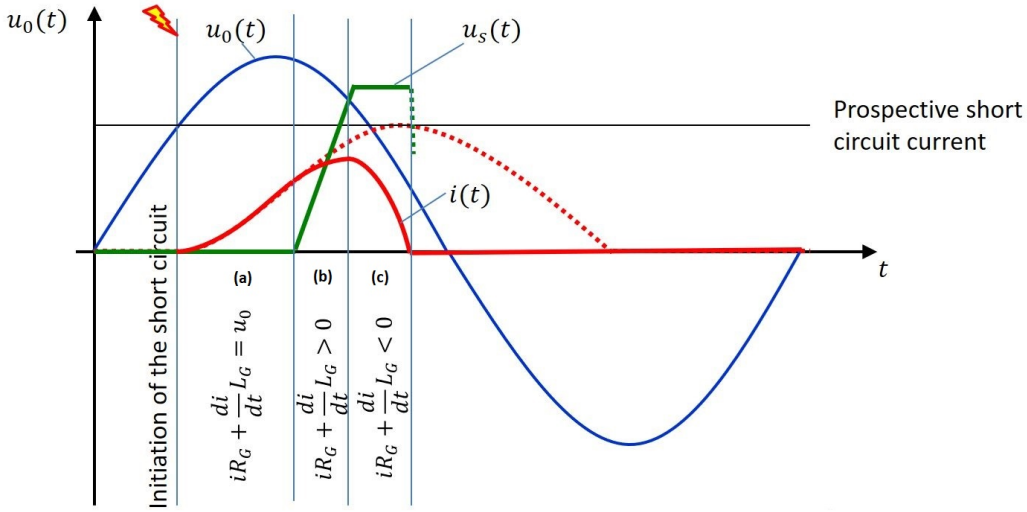

Fig. 2.3: Voltage and current on the ordinate plotted over time on the abscissa [6]

Fig. 2.3 shows the prospective short circuit current that would occur without the counteracting switch voltage $u_s(t)$ as a dotted red line and the actual behaviour of the current $i(t)$ with the counteracting switch voltage $u_s(t)$. According to equation 2.1, when $u_s(t)$ becomes greater in magnitude as $u_0(t)$, the magnitude of the current has to decrease. This behaviour is shown in section (c) in Fig. 2.3. The increase of $u_s(t)$ is mainly caused by the splitter plates of the arc chute.

In case of an electric arc between the separated electrodes the arc will be driven into the arc chute because of the Lorentzforce which is defined as

$$\vec{F} = I \cdot (\vec{l} \times \vec{B}) \qquad [2.2]$$

where $\vec{F}$ is the resulting force vector, I stands for the absolute value of the current, $\vec{l}$ represents the direction of the current flow and $\vec{B}$ represents the magnetic field caused by the current flowing through the electrodes and the arc [4]. Taking a look at a point in time when the voltage is directed as $u_s(t)$ indicates in Fig. 2.1, then the current flows as indicated by the black arrows. Considering the current flow in the current path, the right hand rule describing the induction of a magnetic field and equation 2.2 the resulting force vector acting onto the arc will point into the direction of the arc chute.

In zone 2 of the circuit breaker the arc is lengthened. The arc is also cooled by the gassing lateral walls which decreases the cross section A and reduces the arc plasmas conductivity σ significantly [4]. By definition, the resistance of any conductor can be calculated by

$$R = \frac{l}{\sigma \cdot A} \qquad [2.3]$$

with l being the length, which means that the resistance of the arc is increased [7].

In zone 3 of the circuit breaker in Fig. 2.1 the so-called splitter plates are located. The arc is split up into a number of series arcs by these splitter plates.

This whole arc extinguishing process is influenced significantly by gas dynamic processes, temperature and pressure gradients. In order to obtain more detailed knowledge about how a pressure wave, for example, that is caused by the arc itself when it emerges, influences the propagation behaviour of the arc the pressure distribution may be visualized and quantified.

2.2 Physical Principles

2.2.1 Definition of Light

The phrase light, which is commonly used, refers to the visible light spectrum. This spectrum corresponds to wavelengths between 380 and 760 nm or violet to red light, respectively or white light. White light consists of all these wavelengths. The full spectrum of light reaches from gamma rays with a wavelength of less than 10^{-14} m to long radio waves with more than 10^4 m wavelength. This spectrum is illustrated in Fig. 2.4.

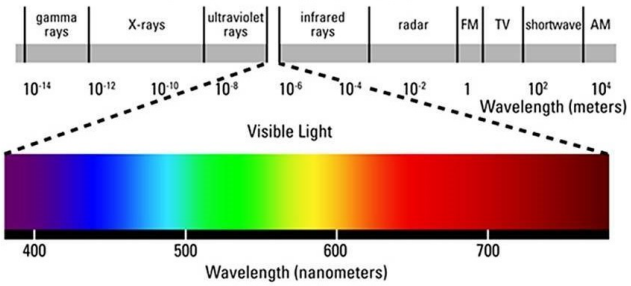

Fig. 2.4: Frequency spectrum of light [8]

According to the measurement methods discussed above, non-visible light will not be of any concern. The speed of light c_0 is a crucial natural constant in physics and in many other technical fields of

studies. While its speed in vacuum is $299.6 \cdot 10^6 \ \frac{m}{s}$, its speed in any other matter with higher optical density is slower. This relationship is given by the index of refraction n which is

$$n = \frac{c_0}{c}, \tag{2.4}$$

where c_0 is the speed of light in vacuum and c the speed of light in matter [7]. As a result, the refraction index is also dependent on the wavelength of the light.

2.2.2 Wave Nature of Light

Light is a transverse, electromagnetic wave [7]. It can be described by the following parameter:

- by its frequency f $[Hz]$ or wavelength λ $[nm]$ which corresponds to its color
- by its intensity I $[\frac{W}{m^2}]$ which describes the spatial energy density at specific locations
- by the propagation vector $\vec{k}$ $[\frac{1}{m}]$ or the Poynting vector $\vec{S}$ $[\frac{W}{m^2}]$ which is defined as

$$\vec{S} = \vec{E} \times \vec{H} \tag{2.5}$$

  while the electromagnetic field vector $\vec{E}$ and the magnetic field vector $\vec{H}$ are defined as shown in Fig. 2.5.

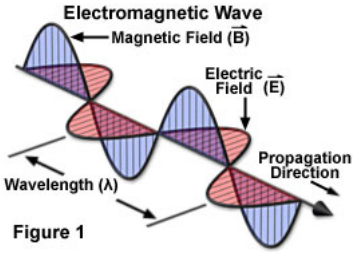

Fig. 2.5: Electromagnetic wave [9]

  It should be noted that $\vec{E}$ and $\vec{H}$ are always perpendicular.

- by its polarization which describes in which direction the waves oscillate. The fields of linear polarized light only oscillate in a single direction, while the fields of circular or elliptical polarized light constantly rotate in a plain as long as the light travels.
- by its phase velocity v_p which is defined as

$$v_p = \frac{\lambda}{T} \tag{2.6}$$

  with λ being the wavelength and T being the period. The phase velocity describes how fast the phase of a wave propagates in space. It should be noted that the phase velocity can be faster than the speed of light in vacuum but this does not mean that a superluminal energy transfer is possible, since the energy transfer happens with the group velocity which is limited to the speed of light.

– whether it is monochromatic and polychromatic which refers to the frequency of light. While monochromatic means that only one certain frequency is present, polychromatic means that more than one frequency is present. Light emitted by the sun or any other light source is, without any further modifications, always polychromatic. For example, a HeNe-laser emits almost only light with a wavelength of 632.8 nm which is achieved by a special application of helium and neon gas [7].

2.2.3 Refraction

If light travels from optical thin to optical dense matter or from optical dense to optical thin matter, it is deflected with respect to the surface orientation. This phenomenon is called refraction [7].

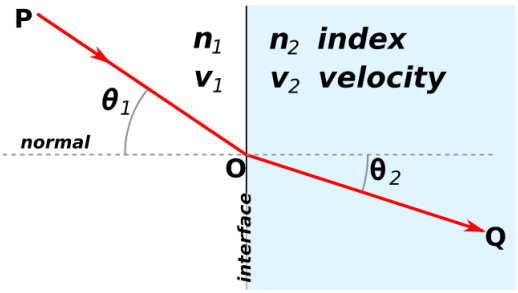

Fig. 2.6: Light travelling from optical thin to optical dense matter [10]

Fig. 2.6 shows this effect for the case from optical thin to optical dense matter. The equation that describes this behavior is called Snell's law[1] and is defined as

$$n_1 \cdot \sin\theta_1 = n_2 \cdot \sin\theta_2, \qquad [2.7]$$

where n_1 is the refractive index of the optical thin matter, n_2 the refractive index of the optical dense matter and θ_1 and θ_2 are defined as shown in Fig. 2.6. It should be noted that if the light impinges right-angled on the surface, no refraction occurs.

2.2.4 Relation between the Index of Refraction, Density and Temperature

In order to obtain a measurement method that can provide quantitative pressure data, the Gladstone-Dale law can be used to establish a relationship between the refractive index and density. It combines the index of refraction n, the density ρ $[\frac{kg}{m^3}]$ and the Gladstone-Dale coefficient K_{GD} $[\frac{m^3}{kg}]$ with the simple equation

$$n = 1 + K_{GD} \cdot \rho, \qquad [2.8]$$

whereas K_{GD} is defined as

$$K_{GD}(\lambda) = 2.2244 \cdot 10^{-4} \cdot \left[1 + \left(\frac{6.7132 \cdot 10^{-8}}{\lambda}\right)^2\right] \qquad [2.9]$$

[1] Snell's law named after William Snellius (1580–1626); originally described first by the Persian scientist Ibn Sahl (c. 940–1000) at the Bagdad court in 984 A.D.

[11]. Assuming that white light is used in the following tests and setups, $K_{GD}(\lambda)$ only varies between $K_{GD}(380\ nm) = 2.2938 \cdot 10^{-4}\ \frac{m^3}{kg}$ and $K_{GD}(760\ nm) = 2.2418 \cdot 10^{-4}\ \frac{m^3}{kg}$. As a result of this, the change of the Gladstone-Dale coefficient is negligible, which is why equation [2.8] is often written as

$$\frac{n-1}{\rho} = constant. \tag{2.10}$$

In order to obtain not only quantitative pressure data but also temperature data, the molar form of the ideal gas law can be used to relate density to temperature. This equation of this law is

$$P = \rho \cdot R_{specific} \cdot T, \tag{2.11}$$

whereby P is the absolute pressure of gas in $[kPa]$, ρ the density in $[\frac{kg}{m^3}]$, T the absolute temperature in $[K]$ and $R_{specific}$ the specific gas constant in $[\frac{J}{kg \cdot K}]$ [7]. For air $R_{specific}$ is equal to 287.058 $[\frac{J}{kg \cdot K}]$.

2.3 Cross-correlation

Cross-correlation is a method to find the similarity of two signals and is defined as

$$f(x) \circ k(x) = \int_{-\infty}^{\infty} f(u) \cdot k(x+u)\ du \tag{2.12}$$

for one dimension, where $\circ$ is the operator to represent the cross-correlation, $f(x)$ and $k(x)$ are signals and u is the shift [12]. For digital image processing the more interesting form of this equation is the discrete form, which is defined as shown in equation [2.13] for one dimension and in [2.14] for the two-dimensional case [13].

$$f(x) \circ k(x) = \sum_{u=1}^{L} f(u) \cdot k(x+u) \tag{2.13}$$

$$\mathbf{F}(x,y) \circ \mathbf{K}(x,y) = \sum_{u=1}^{L} \sum_{v=1}^{W} \mathbf{F}(u,v) \cdot \mathbf{K}(x+u, y+v) \tag{2.14}$$

$f(x)$ and $k(x)$, shown in Table 2.1 and Table 2.2, correspond to one-dimensional signals, whereas $\mathbf{F}(x,y)$ and $\mathbf{K}(x,y)$ correspond to two-dimensional signals, L equals the length of $f(x)$ or the number of columns of $\mathbf{F}(x,y)$ and W equals the width or the number of rows of $\mathbf{F}(x,y)$.

Cross-correlation is an algorithm to calculate a number that is proportional to the similarity of two signals. The calculation works as following:

9	6	4

Table 2.1: $k(x)$

5	2	6	9	6	4	7	8	5	9	1

Table 2.2: $f(x)$

The signal $k(x)$ is a section of the longer signal $f(x)$. As shown in Table 2.3 and Table 2.4, the signal $k(x)$ is shifted from left to right and each corresponding cross-correlation value equals the sum of the multiplication of two overlapping cells. The value of the first step ($u = 1$) equals

9	6	4								
	5	2	6	9	6	4	7	8	5	9	1

Table 2.3: First step of the cross-correlation algorithm

9	6	4								
	5	2	6	9	6	4	7	8	5	9	1

Table 2.4: Second step of the cross-sorrelation algorithm

$$f(x) \circ k(x) = 5 \cdot 4 = 20 \quad [2.15]$$

and the second step ($u = 2$) equals

$$f(x) \circ k(x) = 5 \cdot 6 + 2 \cdot 4 = 38. \quad [2.16]$$

Executing this algorithm for the full length of the signal $f(x)$ yields the results as shown in Table 2.5.

20	38	81	90	132	133	106	110	131	138	103	87	9

Table 2.5: Result of the cross-correlation algorithm with the signals $f(x)$ and $k(x)$

In order to find the position of $k(x)$ in $f(x)$ the autocorrelation must be calculated. This is done by computing the cross-correlation algorithm of $k(x)$ with itself. This computation yields the results as shown in Table 2.6.

36	78	133	78	36

Table 2.6: Result of the autocorrelation of $k(x)$

The maximum autocorrelation value of $k(x)$ is 133 which can also be found in Table 2.5 at position $u = 6$. At this particular position $k(x)$ exactly matches $f(x)$.

This algorithm may be extended to two dimensions easily since the calculation is simply repeated for each row which results in a two-dimensional matrix as shown in Table 2.9.

8	2	3
5	6	4
2	7	6

Table 2.7: Matrix $\mathbf{K}(x, y)$

7	8	2	3	5	2
8	5	6	4	1	7
4	2	7	6	4	8
1	7	9	6	5	7
5	9	2	4	1	6

Table 2.8: Matrix $\mathbf{F}(x, y)$

42	97	82	48	55	53	24	4
76	160	178	140	94	110	88	24
77	146	236	243	175	182	155	67
46	112	257	253	236	230	149	110
46	137	225	217	219	219	159	111
23	89	136	165	137	129	95	86
15	37	64	88	27	52	20	48

Table 2.9: Result of equation [2.14]

The bottom right corner of $\mathbf{K}(x, y)$, as shown in Table 2.7, is represented by number 6 in this example and hence overlaps with the top left corner of $\mathbf{F}(x, y)$, as illustrated in Table 2.8, which has

the number 7 at this position. This multiplication, of course, yields the number 42 which is positioned in the top left corner of the resulting table illustrated in Table 2.9. After finishing this row, the bottom right corner of $\mathbf{K}(x, y)$ is shifted to the next row and the algorithm is executed again.

The maximum autocorrelation value of $\mathbf{K}(x, y)$ is 243 which again yields the position of $\mathbf{K}(x, y)$ in $\mathbf{F}(x, y)$ at $u = 3$ and $v = 4$. Additionally, it is essential to consider that the autocorrelation value does not need to be the highest value, since the highest value depends on the brightness and intensity of the picture. The cross-correlation algorithm is a very powerful tool to find similarities or exact subsections of one image in another.

3 Schlieren Imaging Setups

3.1 Single-Lens Schlieren System

By applying some of the previous principles, August Toepler[1] was the first to investigate liquid or gaseous flow. Such a setup is known as Toepler's single-field-lens schlieren system and is illustrated in Fig. 3.1 [14].

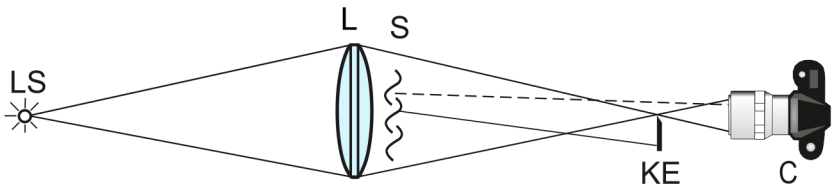

Fig. 3.1: Toepler's single-field-lens schlieren system. Reproduced from [15] by permission of Dr. G. S. Settles

The light source LS emits divergent light which is refracted and focused by the biconvex lens L. Behind the lens L a change of refractive index of any form is present, which refracts the light again. The purpose of the knife-edge KE is to cut off the part of the light that is deflected. In order to do so, the knife-edge has to be placed exactly at the focal point of the lens. Some light rays may be deflected, pass above the cutoff, and illuminate any parts of the schlieren image that is captured with the camera C as shown in Fig. 3.1. The light beam that is deflected in a way that makes it impinge on the cutoff creates spots with less brightness on the captured picture [1]. This setup is an effortless way to display schlieren qualitatively. However, some disadvantages can be encountered when it comes to quantitative evaluation. Since the light is converging when it travels through the schlieren streaked matter the result is falsified and more effort is needed to extract correct quantitative data.

3.2 Dual-Lens Schlieren System

Because of the problem with the converging beam the more commonly used setup is the dual-lens schlieren system as shown in Fig 3.2 [1].

The major difference between these two setups is that when the light gets deflected by the schlieren streaked matter it is no longer convergent but collimated. This arrangement improves the accuracy and facilitates obtaining quantitative data. Another difference to the single-lens system is that in this arrangement the lenses are achromatic and not biconvex. These types of lenses decrease the dispersion

[1] August Joseph Ignaz Toepler (* 7 September 1836 – 6 March 1912), German physicist

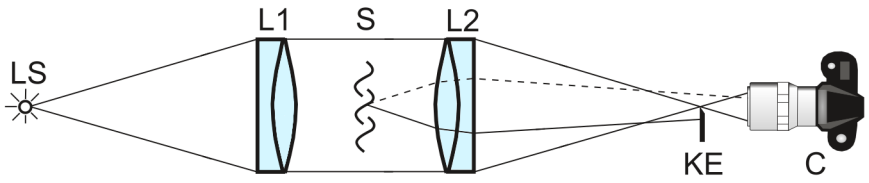

Fig. 3.2: Dual-lens schlieren system. Reproduced from [15] by permission of Dr. G. S. Settles

of the focal point and sharpen the resulting schlieren image. The lenses which are required for the single-lens as for the dual-lens system can be, depending on the diameter, highly expensive [1].

3.3 Background-Oriented Schlieren

The so-called Background-oriented Schlieren technique (BOS) is the simplest way to visualize the changes of the index of refraction, which is illustrated in Fig. 3.3 [1].

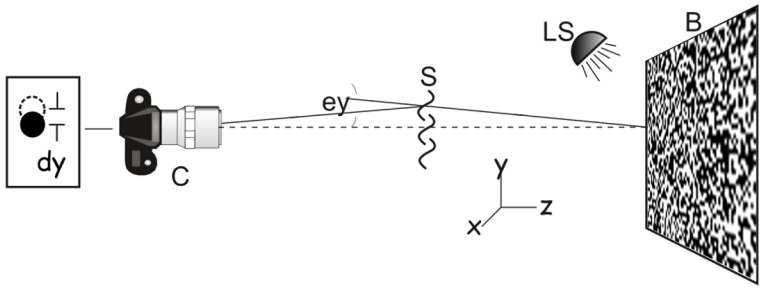

Fig. 3.3: Background-oriented Schlieren setup with random dot pattern background. Reproduced from [15] by permission of Dr. G. S. Settles

This system is based on the same principle as the other two systems with the exception that the schlieren do not cause a shadow on the background. Instead, BOS utilizes an optical shift dy of the background on the image sensor which is caused by schlieren streaked matter [15]. By placing a certain pattern in the background, as it was done with the random dot pattern in Fig. 3.3, and taking two pictures, the shift can be visualized easily. In order to provide a reference image the first image needs to be taken when no schlieren are present. The second image must be taken without any changes of the position of the camera or the background; only the schlieren may be placed between the camera and the background. The visualization is achieved in the post processing by subtracting the reference picture from the distorted picture with any capable image processing software.

4 Scientific Quesiton

In general, both, the dual-lens system and the Background-oriented Schlieren (BOS) system are suitable for arc filming. While Background-oriented Schlieren is more suitable when the arc is not fully accessible from all perspectives, dual-lens and dual-mirror systems require full accessibility. Regarding the evaluation and quantification of the pictures, both options require post-processing including an appropriate software and additional effort in mathematics. Available MATLAB™ functions or already existing scripts may be used for the quantification. MATLAB™ may be used to post-process the acquired images and quantify the temperature and pressure two-dimensionally as it offers an extensive selection of image processing functions. With MATLAB™ and the open source software OpenPIV the offset vectors of subsections of the distorted image compared with the reference image may be calculated. Information about whether a Background-oriented Schlieren system, a dual-lens or a dual-mirror system suits best the requirements for the desired application best must be examined by appropriate literature. Eventually, a suggestion for an appropriate schlieren system has to be made with respect to the special requirements laid down by the application to evaluate electric arcs. In order to use BOS or a dual-lens system for the investigation of an electric arc in a circuit breaker, the two gassing lateral walls would have to be replaced by glass. For Background-oriented Schlieren the glass is necessary to enable the view to the background pattern behind the circuit breaker. For a lens system the glass is necessary to allow the light beam to pass through. The question to be answered is whether Background-oriented Schlieren is appropriate to resolve schlieren with a simple camera or not. The lower resolution of a high-speed camera of 1024×1024 pixels or less has to be considered. Furthermore, it should be ascertained if a color camera could be of advantage and which setup would be proposed for a test.

5 Approach

For convenience only, it was determined that only Background-oriented Schlieren (BOS) tests will be implemented as setting up an entire dual-lens or dual-mirror system requires a high amount of optical equipment which would exceed the budget of this research. Then, the framework conditions for taking the best possible Background-oriented Schlieren photos were set out. Furthermore, it needs to be determined if special backgrounds are required for the quantitative evaluation. If this is the case, it is essential to state which backgrounds provide the best results.

6 Tests and Results

6.1 Setup

The Background-oriented Schlieren tests were conducted with available equipment such as:

- The rear camera of an Xiaomi Mi5 smartphone as camera
- Tripod Fotopro FY583 to mount the smartphone
- Bluetooth remote trigger to trigger the camera
- Projector Dell™ 2300MP
- Butane lighter to create schlieren with its flame
- Different background patterns (printed and projected)

6.1.1 Camera

The used camera of the smartphone Xiaomi Mi5 had a resolution of 16 MP and a f/2.0 aperture. This camera has a much higher resolution than the actual High-Speed camera Photron FASTCAM APX-RS, shown in Fig. 6.1, at desired frame rates, but the principle of the processing and evaluating is the same. Although, the loss of information due to lower resolution must be taken into account.

Fig. 6.1: High-speed camera Photron APX-RS [16]

6.1.2 Tripod

The tripod Fotopro FY583, as shown in Fig. 6.2, was used in order to provide a stationary position for the camera which was crucial for this setup. The camera mounted on the tripod with the included smartphone mount shown in Fig. 6.3 was placed on a table and remained unmoved, as far as this was possible, during taking the reference and the distorted picture.

Fig. 6.2: Tripod Fotopro FY583 [17]

Fig. 6.3: Smartphone mount [18]

6.1.3 Bluetooth Remote Trigger

The Bluetooth remote trigger, which was included when buying the tripod, was used in order to prevent blurring and to improve the quality of the images.

6.1.4 Projector

The projecter Dell™ 2300MP was used to project the pattern onto the wall in the first test setup. It is shown in Fig. 6.4.

Fig. 6.4: Projector Dell™ 2300MP [19]

6.1.5 Butane Lighter

A simple butane lighter flame was used to create the schlieren between the camera and the background. The flame itself is not visible on the images since the lighter was fixed beneath the captured picture of the background, as illustrated in Fig. 6.9.

6.1.6 Background Pattern

The used background pattern is, as simple as it seems, the key factor when it comes to quantitative evaluation. "The tests show that size and spacing of the background pattern are the primary attributes for pattern optimization while shape of the pattern does not impact image quality" [11]. Two different pattern designs including various sizes of each pattern were tested. The first pattern was a random dot pattern, as shown in Fig. 6.5 and Fig. 6.6.

The second pattern was generated with the MATLAB™ function `rand([M, N])` which returns a $M \times N$ matrix filled with numbers between 0 and 1. The resulting matrix was converted to a black and white image by using the function `im2bw(matrix)` which converts values less than or equal to 0.5

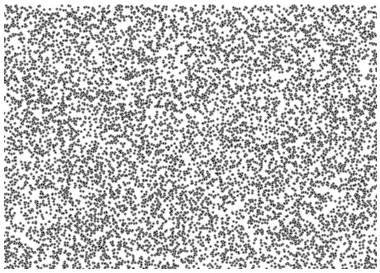

Fig. 6.5: Random dot pattern in original size [20]

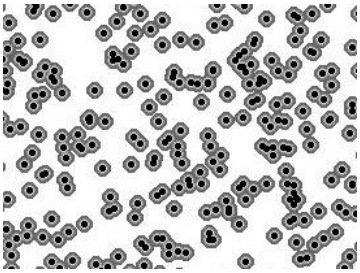

Fig. 6.6: Fig. 6.5 magnified

to 0 and all other values to 1. The result for $M = 50$ and $M = 500$ rows is demonstrated in Fig. 6.7 and Fig. 6.8.

Fig. 6.7: Result for M = 50

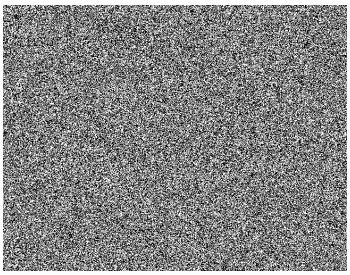

Fig. 6.8: Result for M = 500

The calculation of the value for N was based on the available printing paper which was an 8.5×11 inch letter paper. The resulting factor was approximately $\frac{11in}{8.5in} = \frac{279.4mm}{215.9mm} = 1.29412$. The calculated number of columns was rounded by using the MATLAB™ function `round(decimal)` which rounded to the nearest integer.

6.1.7 Setup Background-Oriented Schlieren with Projector

Fig. 6.9 illustrates the arrangement in case of the projector projecting the pattern onto the wall.

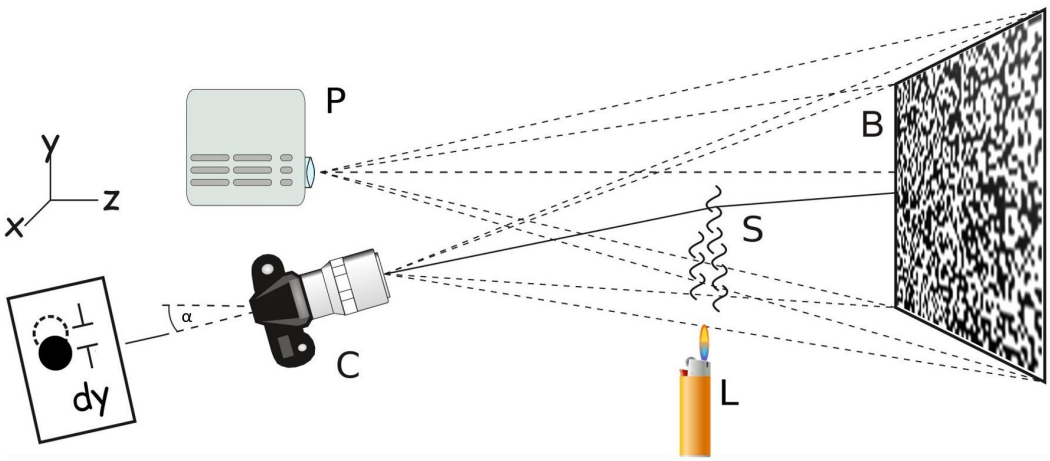

Fig. 6.9: Test setup with the projector, the camera and a butane lighter

The lighter L was fixed low enough in order to be invisible in the schlieren photos. Consequently, the distorted area which was captured was maximized. The offset angle α between the camera and

the surface orientation of the wall was held small with a magnitude of about 3 to 5°.

6.2 First Test Setup: Projected Pattern

For the first test the video projector was used to project the pattern onto the wall. As shown in Figure 6.10 and in Fig. 6.11, the differences are not accessible by watching the patterns only, but when using the MATLAB™ function `imsubtract(X,Y)` the distortion may be visible.

6.2.1 Experiment 1

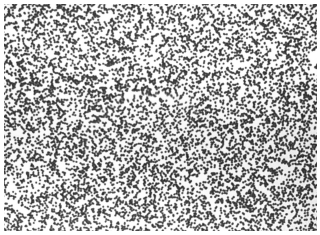

Fig. 6.10: Reference image

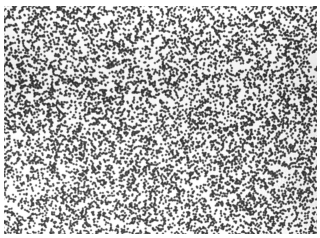

Fig. 6.11: Distorted image

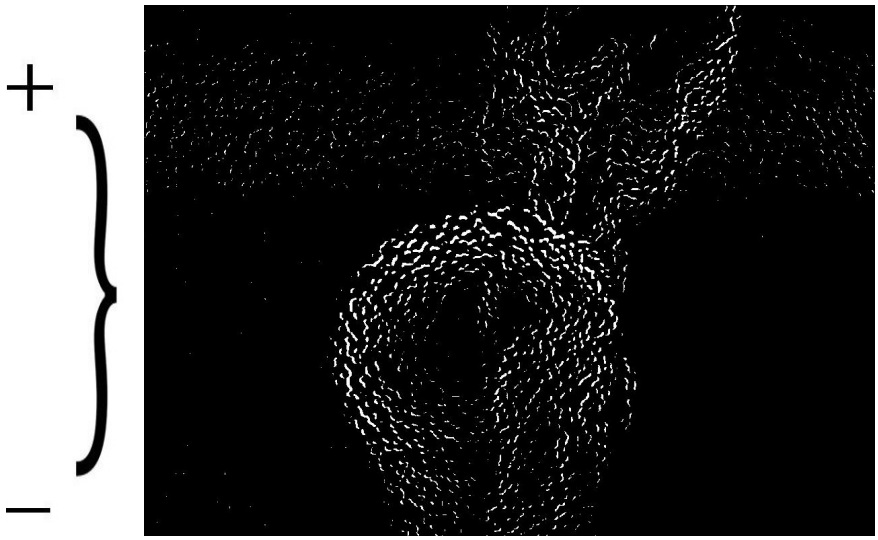

Fig. 6.12: Difference image converted to a black and white image

The distorted photo, which is presented in Fig. 6.11, was exactly taken when the lighter was lit. This resulted in a circular turbulent gas flow which is indicated by Fig. 6.12. Due to the fact that an image consists of a matrix with data about the brightness of each element, this function simply subtracts each value of the image Y from the value of the corresponding element of the image X. The value 0 corresponds to black and 1 to white. All values in between are interpreted as grayscale. In order to enhance the difference for the reader the difference image was also converted to a binary image with a threshold of 0.2. A binary image is basically the same as a grayscale image with the exception that it does not allow any other values than 0 or 1. The threshold of 0.2 means that all values above 0.2 are interpreted as white and every value below as black. This function helps to visualize the difference for the human eye but impairs the ability to evaluate the difference numerically.

The reference and the distorted image were processed with the open source software OpenPIV[1] in order to make it possible to calculate the temperature and density field caused by the lighter flame. In principle, this software uses the cross-correlation algorithm and detects similar or equal subsections of two images. The software allows to select the size of the interrogation window which influences the accuracy of the result.

Depending on the setting of the interrogation window size and the power of the computer, the calculation of the offset vector can take some time. For the calculation of the offset vectors, as shown

[1] PIV stands for **P**article **I**mage **V**elocimetry

in Figure 6.13, the interrogation window size was set to 32 x 32 pixels and the Spacing/Overlap to 16 x 16. The used S/N^2 filter type was type 2 with an S/N value of 1 and the outlier filter was set to 10. The meaning of these parameters is described on the OpenPIV-Homepage [21].

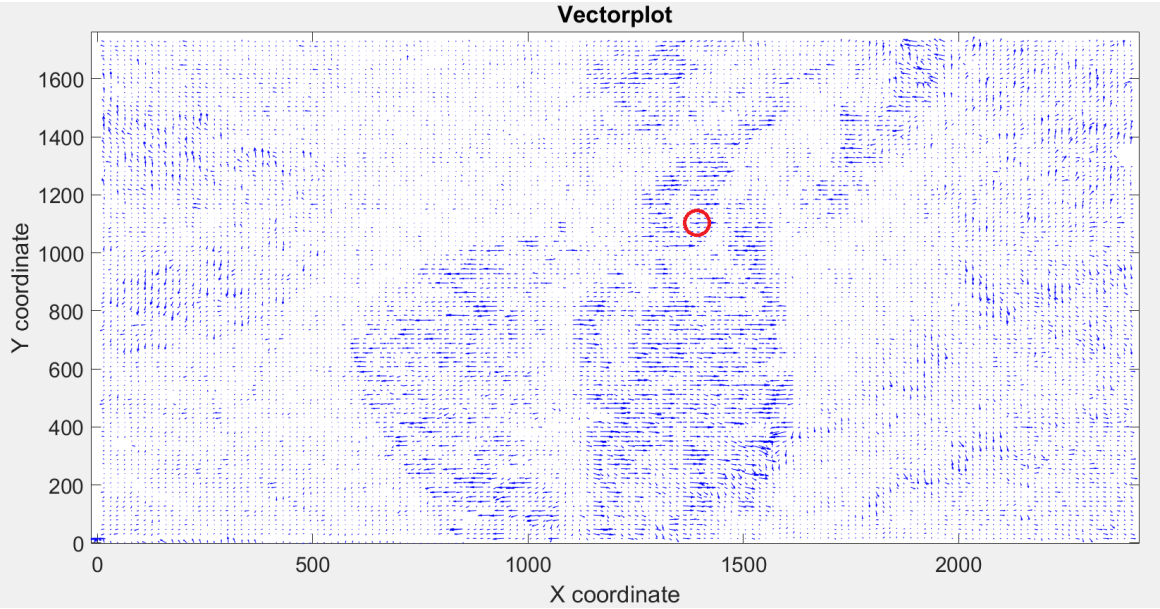

Fig. 6.13: Vectorplot of the result of the first experiment

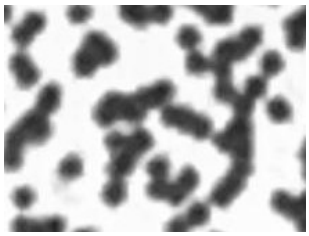

Fig. 6.14: Magnified section of the background captured during the first experiment

The vector plot of the result of the first experiment shows a certain change in the right area which is, however, not good enough to gain consistent, quantitative data. The magnified image in Fig. 6.12 shows that the dots from the distorted image of the original random dot pattern, shown in Fig. 6.5, are blurred. The reason for this blurring was due to a problem with the autofocus. This leads to a loss of information and therefore makes it almost impossible for the cross-correlation algorithm to find corresponding sections.

6.2.2 Experiment 2

As a result, a second trial was attempted with more concentration on the right focus. The resulting vectorplot and difference image from this second attempt are shown in Fig. 6.15 and Fig. 6.16, respectively.

Obviously, the magnitude of the offset vectors is longer within the temperature field which is caused by the lighter flame, as shown in Fig. 6.15. The difference image, as shown in Fig. 6.16, was first

[2]Signal-to-Noise

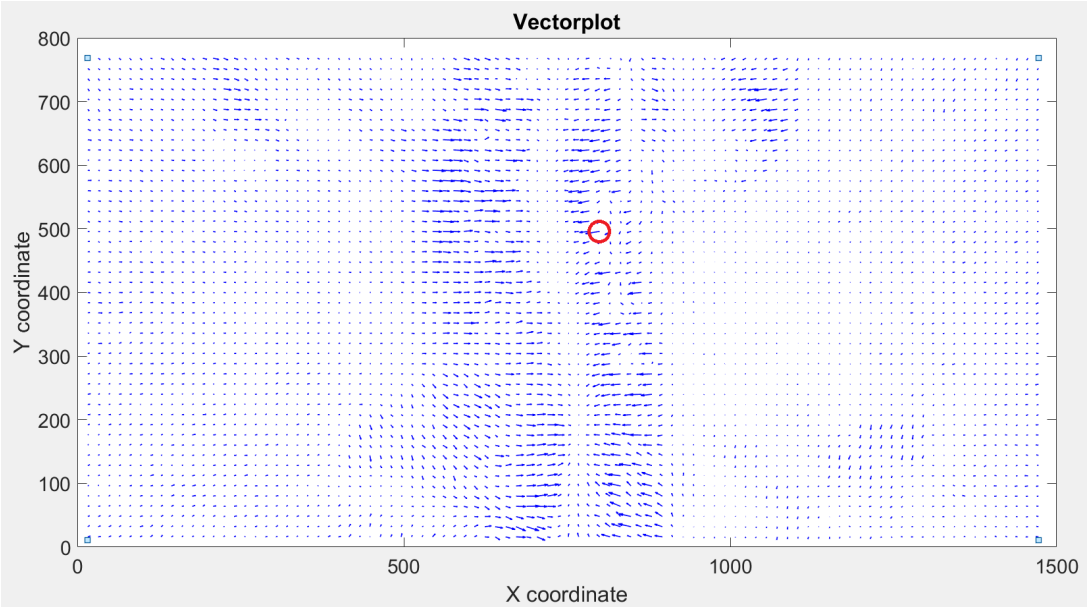

Fig. 6.15: Vectorplot of the result of the second experiment

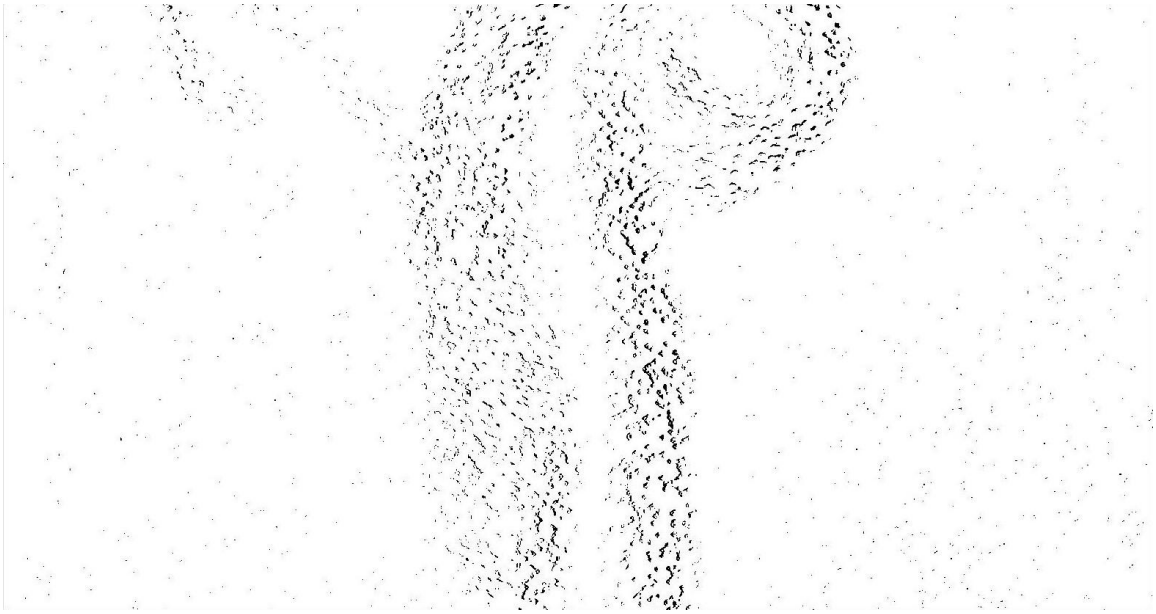

Fig. 6.16: Difference image of the reference and the distorted image taken during the second experiment (converted to black and white with a threshold of 0.2 and complemented afterwards)

converted to a black and white image. In order to improve the reader's recognizability the colors were inverted afterwards. Hence, this setup does not maintain optimal conditions for investigating arcs and the resulting arc blasts without any further arrangements as it is highly sensitive to vibrations. OpenPIV has a built-in function to filter some of these outliers which compares the actual vector with its neighbors, because only a continuous and not an abrupt change in temperature is possible.

The result of the second experiment is noticeably better. Apart from this one good result, projecting the background by the projector caused numerous problems. One of these problems are the horizontal color stripes, as shown in Fig. 6.17.

These stripes occur because of the close frame rate of the projector and the shutter synchronization

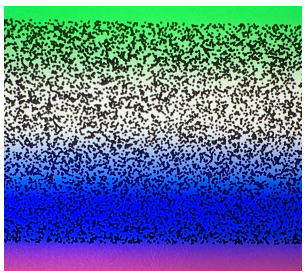

Fig. 6.17: Color stripes caused by wrong recording frequency

with camera. This problem could be avoided by synchronizing the shutter time of the camera so that it captures an entire cycle of the projected image. This kind of adjustment was not possible with the camera of the used smartphone.

Another disadvantage of this system is the high sensitivity to vibrations since the camera and the background are moveable. A slight displacement of the projector causes invalidation of the captured information. An even greater disadvantage of this setup is the possible appearance of schlieren in all sides of the object. This means that the object needs to be placed in the middle of the image. Hence, the background disappears and makes the evaluation of the area close to the object impossible. Because of these reasons, this setup is not suitable for the desired application.

6.3 Second Test Setup: Printed Pattern

In order to eliminate of the sensitivity to vibrations and the color stripes, it is essential to use printed patterns. For these tests, the patterns shown in Fig. 6.5 and 6.7 were used. The pattern shown in Fig. 6.7 was printed with a different number of rows M which were 10, 50, 100, and, 500. The best result was obtained by the subtraction of Fig. 6.19 from Fig. 6.18 with 500 rows. The result of this subtraction is shown in Fig. 6.20.

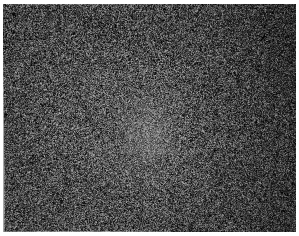

Fig. 6.18: Reference image

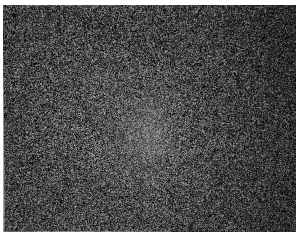

Fig. 6.19: Distorted image

Fig. 6.20: Difference image converted to a black and white image and inverted colors

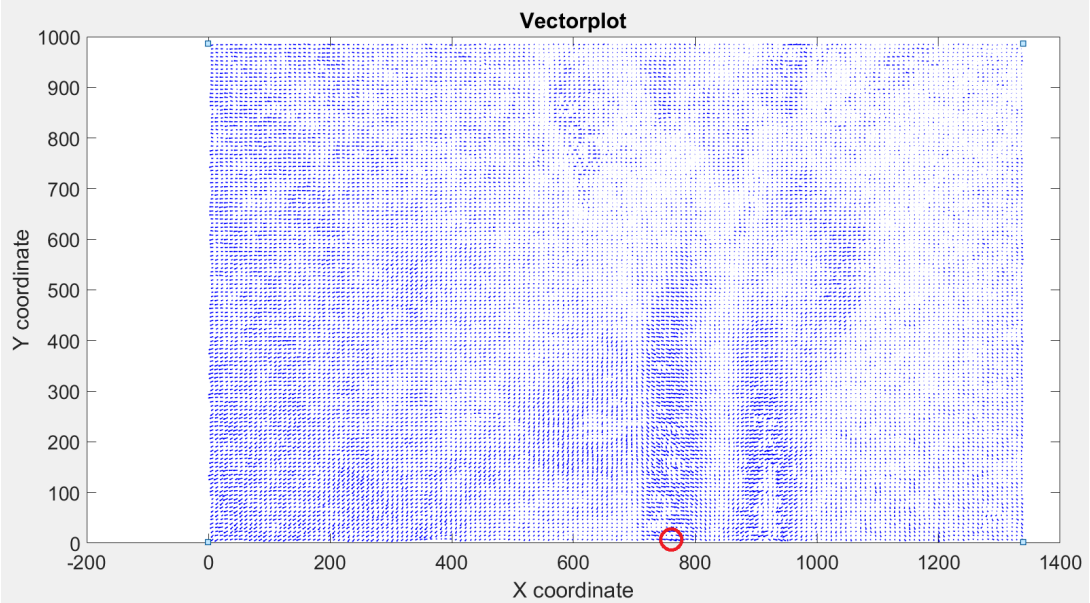

Fig. 6.21: Plotted offset vectors between the reference image Fig. 6.18 and the distorted image Fig. 6.19.

Due to non-ideal conditions during the test, which includes instability of the table and the tripod, the left half of the vector field in Fig. 6.21 indicates a continuous change in temperature. To avoid this misinterpretation, the left part of the image could simply be cut off. In contrast to the projected

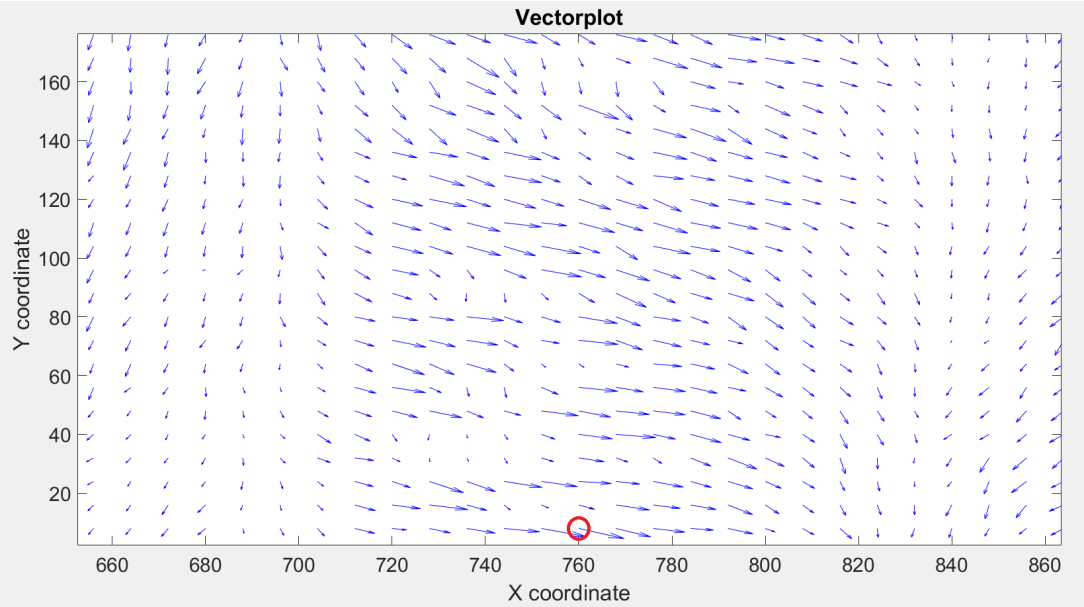

Fig. 6.22: Magnified area of Fig. 6.21 with the longest occurring vector in it

pattern setup, this setup yielded a series of appropriate images. Hence, the attempt of quantitative evaluation was based on this type of setup.

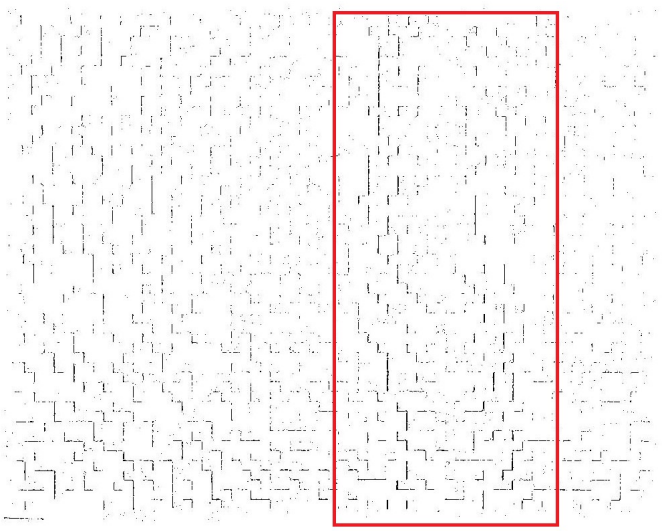

Fig. 6.23: Result of the subtraction with M = 50 rows

The post-processing quickly showed that less dots in the background also means less data. An example is shown in Fig. 6.23 where the background had 50 rows. It is qualitatively detectable that a change of the index of refraction occurred. However, it is not suitable to provide quantitative data for an evaluation of temperature and density distribution in the area of interest.

6.3.1 Evaluation

"Specifically, according to Venkatakrishnan and Meier [22], the relationship between background-element displacement and refractive index gradient of the disturbed flow field is given by

$$\Delta x = \frac{Z_D \cdot Z_I}{Z_B} \cdot \int_{Z_D-\Delta Z_D}^{Z_D+\Delta Z_D} \frac{\partial n}{\partial x} dz, \qquad [6.1]$$

and

$$\Delta y = \frac{Z_D \cdot Z_I}{Z_B} \cdot \int_{Z_D-\Delta Z_D}^{Z_D+\Delta Z_D} \frac{\partial n}{\partial y} dz, \qquad [6.2]$$

where Δx and Δy are the background-element displacements in the horizontal direction (i.e., the x-axis direction) and vertical direction (i.e., the y-axis direction), respectively; Z_D is the distance from the background to the centre of a disturbed flow field; Z_B is the distance from the background to the lens; Z_I is the distance from the lens to the imaging plane; ΔZ_D is half of the thickness of the disturbed flow field; n is the refractive index inside the disturbed flow field; n_0 is the refractive index of the undisturbed flow that is measured before the experiment; and z is the line-of-sight direction" [23]. These parameters are illustrated in Fig. 6.24.

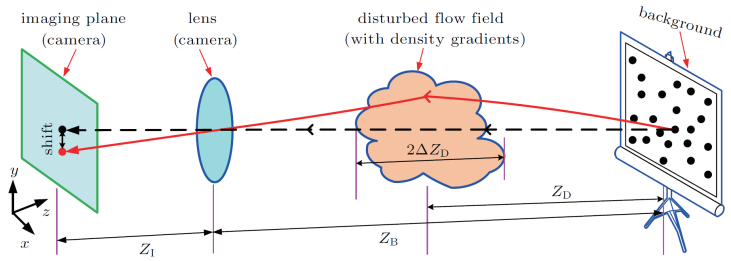

Fig. 6.24: Schematic representation of the background displacement caused by schlieren. Reproduced from [23] by permission of Guang-Ming Guo.

In order to evaluate the quantitative temperature data, Poisson's equation must be solved for the refractive index. The equation is represented by

$$\frac{\partial^2 n}{\partial x^2} + \frac{\partial^2 n}{\partial y^2} = C \cdot \left[\frac{\partial \Delta x}{\partial x} + \frac{\partial \Delta y}{\partial y} \right] \qquad [6.3]$$

where x and y are the directions, C is a constant and Δx and Δy the displacements of the background in each direction. This equation "describes the refraction index distribution in a disturbed flow field" [23]. Solving this equation would be beyond the scope of this paper, so the solution is only described. The full derivation can be found in Guang Ming (2017).

Knowing the distribution of the index of refraction quantitatively, equation [2.8] can be used to obtain the density. By application of equation [2.11] the corresponding temperature field can be calculated. With a self-developed MATLAB™ script it was possible to find the longest vector of this vector field which is highlighted by a red circle in Fig. 6.13, Fig. 6.15 and Fig. 6.21. During the test a ruler was placed in the background which allowed to find a relation between pixels and mm. In the

case of the discussed images Fig. 6.18 and Fig. 6.19, 1 mm corresponded to 7 pixels. This lead to the longest absolute distortion of the background on the image sensor of the camera of approximately 0.1 mm. However, Z_I was not possible to determine for the used smartphone camera. Since the actual calculation of the density and the temperature values was not the aim of this research, it was not of interest any more.

7 Desired Schlieren System for Arc Filming

7.1 Setup

The Background-oriented Schlieren tests showed that this setup is not suitable for a system with high accuracy and reproducibility in a rough environment without any further precautions. However, the tests helped to show and understand the process of obtaining and processing the data. Another schlieren system may be used to investigate arcs. The earlier mentioned Dual-lens system may fulfil these requirements. Another system, which is smaller but operates in the same way is the dual-mirror system. The dual-mirror setup is shown in Fig. 7.1.

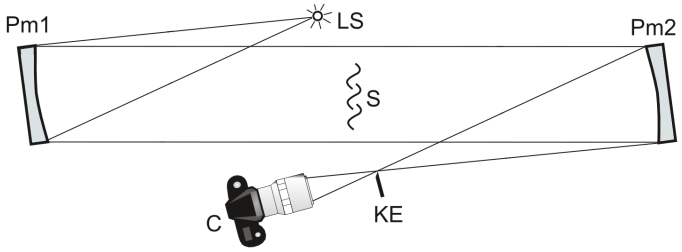

Fig. 7.1: Dual-mirror system. Reproduced from [15] by permission from Dr. G. S. Settles.

7.1.1 Light Source

For the better part of the 20^{th} century, light sources that were used for schlieren photography or any other application which required a point-like light source were light bulbs in combination with a slit or a hole to produce a convergent light source [15]. Due to the fact that LEDs have become cheaper, more powerful and smaller in the last decade, they are qualified for a point-like light source. "The ubiquitous, inexpensive 5 mm T-1$\frac{3}{4}$ LEDs, for example, typically have 1 mm diameter emitters. This is small enough to produce sharp shadowgrams, but not too small to be an effective schlieren lamp" [15]. Fig. 7.2 shows the problem that occurs when not using a point-like light source.

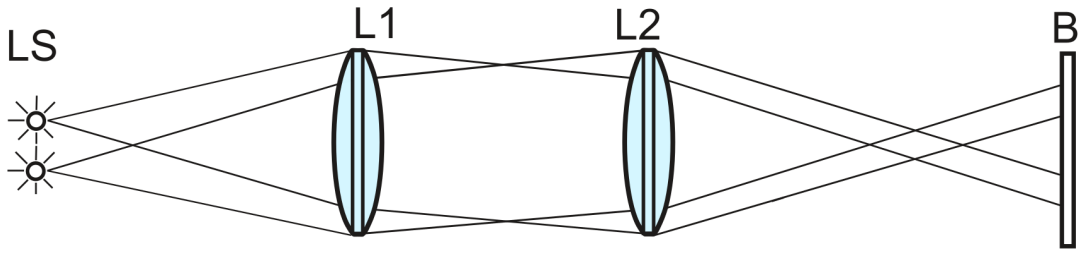

Fig. 7.2: An extended light source creating a blurred image on the background

It results in blurred images and therefore complicates gaining quantitative data of the resulting image.

7.1.2 Lenses

Like light sources, lenses have to fulfil certain requirements in order to yield the best result. According to the problems with lenses, chromatic and spherical aberrations are the issues which need to be dealt with, as shown in Fig. 7.3. A lens that compensates these aberrations is called achromat or achromatic doublet, as illustrated in Fig. 7.4.

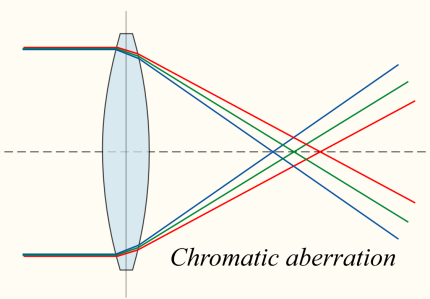

Fig. 7.3: Biconvex lens with chromatic and spherical aberration [24]

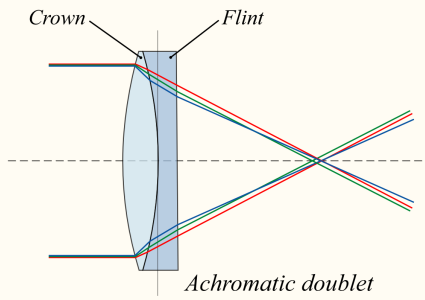

Fig. 7.4: Achromatic lens with the correction of both aberrations [24]

7.1.2.1 Chromatic Aberration

Chromatic aberration is the result of the dependency of the index of refraction on the wavelength. Usually, the index of refraction increases with decreasing wavelength, which is called normal dispersion. This phenomenon is shown in Fig. 7.5 and Fig. 7.6.

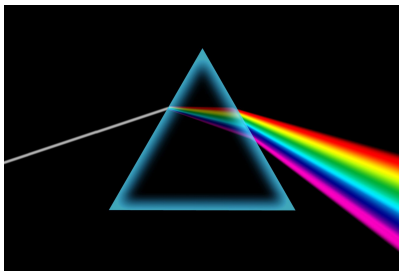

Fig. 7.5: Chromatic aberration of a prism [25]

Fig. 7.6: Chromatic aberration in a photograph [24]

Chromatic aberration causes a color shift and the picture to be blurry. Due to the fact that most light sources emit white light, which consists of all wavelengths and therefore all colors, this effect has to be taken into account when setting up a schlieren system for a quantitative evaluation.

7.1.2.2 Spherical Aberration

Spherical aberration is caused by the spherical surface of the lens which results in focusing the light beam that impinges near the outer edge to have a different focal point than a light beam that impinges near the center of the lens. This effect is shown in Fig. 7.7 and a lens that compensates this aberration, a so-called aspherical lens, is presented in Fig. 7.8.

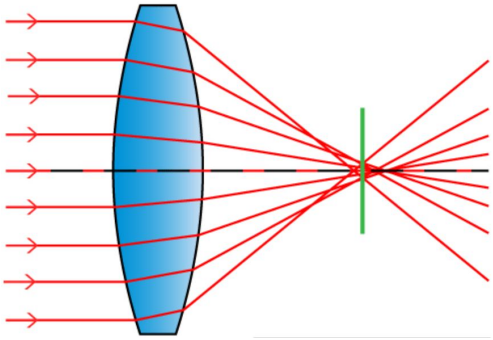

Fig. 7.7: Biconvex lens with spherical aberration [26]

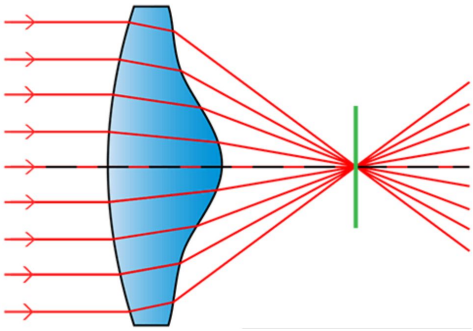

Fig. 7.8: Aspherical lens to correct spherical aberration [26]

7.1.3 Mirrors

Using parabolic mirrors rather than lenses allows the setup to be smaller in length since the light source and the camera have to be positioned one on each side of the setup. This arrangement causes different issues such as coma and astigmatism, as explained subsequently.

Parabolic mirrors are very similar to lenses as far as the operating principle is concerned. The only exception is that the light rays are not focussed on the opposite but rather on the same side they come from, as shown in Fig. 7.9.

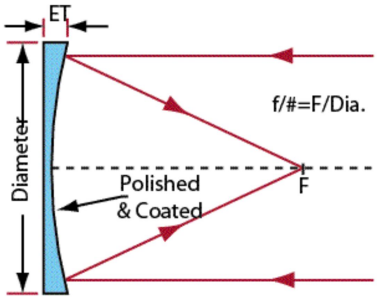

Fig. 7.9: Illustration of the operating principle of a parabolic mirror [27]

7.1.3.1 Coma

Coma occurs when a beam of light impinges at a certain angle on the mirror or lens rather than perpendicularly. The point focus expands to a line which causes a so called ”comet” whose ”tail” is directed away from the optical axis of the mirror or the lens. Fig. 7.10 presents the perspective of one side of this phenomenon whereas Fig. 7.11 shows the front view.

”Coma grows in proportion to the offset angle θ and to the inverse square of the mirror f/no. for a given θ.” [1]. This is the reason why the offset angle should be kept as small as possible, in the order of 2 - 5°. If both mirrors of a dual-mirror system are tilted the exact same angle, as illustrated in Fig. 7.1, the coma eventually cancels out on the resulting image [1].

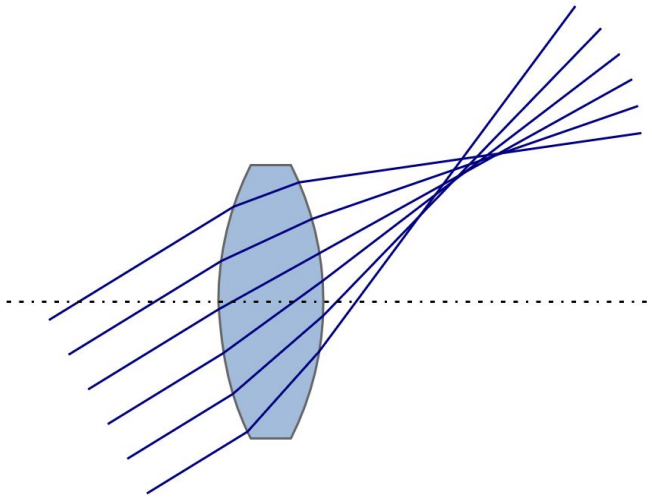

Fig. 7.10: A beam of light impinging oblique on a biconvex lens [28]

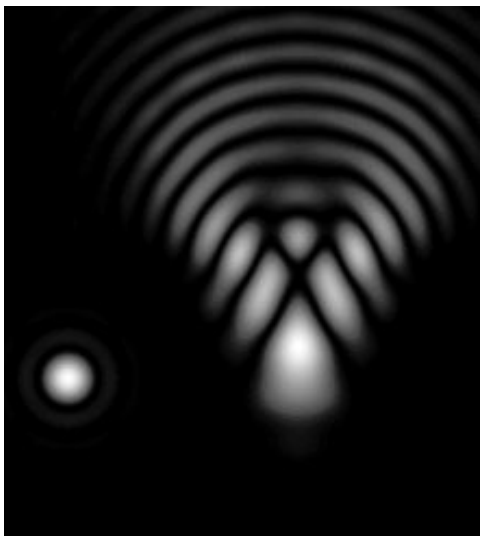

Fig. 7.11: Comparison of the focal points between a perpendicular and an obliquely impinging beam of light [28]

7.1.3.2 Astigmatism

Astigmatism is, like coma, an error of the focal length but it is caused by varying precision in the production and when there are paths for the light beams with different lengths [1]. Astigmatism due to different lens curvatures is shown in Fig. 7.12 and astigmatism due to an unsymmetrical arrangement is shown in Fig. 7.13.

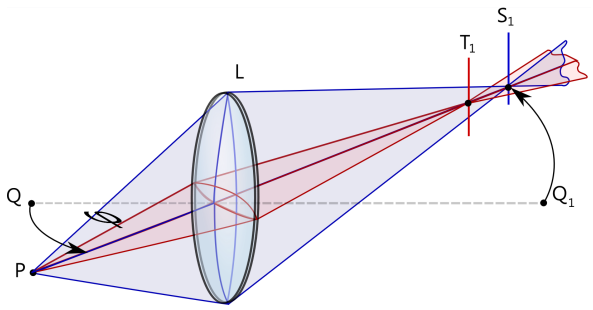

Fig. 7.12: Astigmatism of a light beam caused by a lens [29]

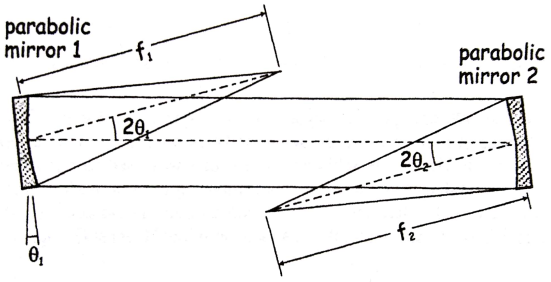

Fig. 7.13: Astigmatism in a Z-type schlieren system. Reproduced from [1] by permission of Dr. G. S. Settles.

In contrast to coma where the focal point smears, astigmatism causes the focal length to change, depending on which plane the light travels through the lens. As shown in Fig. 7.12, light that travels in the horizontal plane is focussed at a different length than light that travels in the vertical plane.

7.1.4 Knife-Edge Cutoff

The Knife-Edge cutoff is an essential part of most schlieren visualizing systems and can be a simple razor blade or a more complex structure as shown in Fig. 7.14.

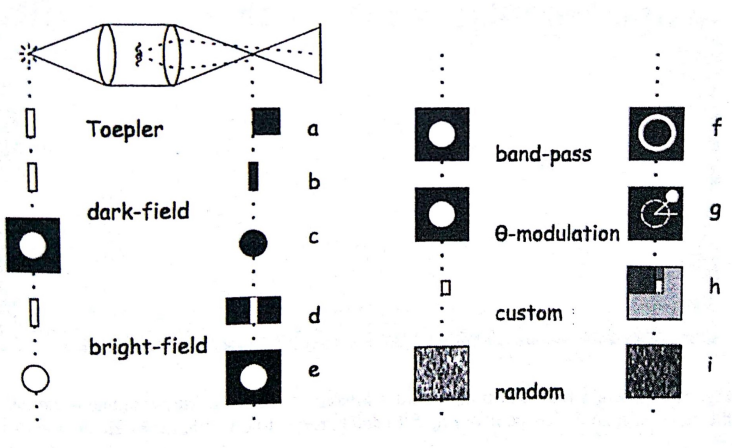

Fig. 7.14: Different cutoffs and filters for schlieren imaging. Reproduced from [1] by permission of Dr. G. S. Settles.

The first cutoff, Fig. 7.14(a), shows the simple setup Toepler used first to visualize schlieren [1]. It consists of a simple slit and a knife-edge. The operating principle of this setup can be re-read in the above chapters. The following cutoffs and filters can be classified in two different categories: bright- and dark-field filters. Fig. 7.14(b) shows a cutoff for symmetric dark-field illumination regarding the horizontal axis. This cutoff filters all light rays which are not deflected but, depending on the width, also some of the deflected ones. Fig. 7.14(c) shows an example for a symmetric dark-field illumination filter with respect to both the horizontal and the vertical axis. Fig. 7.14(d) and Fig. 7.14(e) show a bright-field illumination filter whereas (d) is only symmetrical to the horizontal axis and (e) to both axes. Fig. 7.14(f) is a combination of bright- and dark-field illumination since only light that is deflected and impinges in this certain area is let through. In Fig. 7.14(g) a cutoff for passing light only in a certain direction depending on its radius is illustrated. Fig. 7.14(i) and Fig. 7.14(h) show two completely different filters. (h) represents a color filter which is described more precisely in chapter 6. (i) simply shows a random dot pattern background for Background-oriented Schlieren as was already explained earlier.

Regarding the sensitivity, Settles pointed out that although Toepler's cutoff does not provide a symmetrical schlieren image it does not need as much effort to adjust to high sensitivity as all the other filters do [1]. For this reason, Toepler's cutoff provides the highest possible sensitivity for monochrome schlieren imaging.

7.1.5 Calibration and Quantitative Evaluation

One allegedly easy calibration method was described by Hargather and Settles [3]. They used a calibration lens to establish a relationship between the refraction angle and the pixel image intensity. The used calibration lens must have a long focal length in order to produce refraction angles within the range of interest [3]. This entire calibration process is based on the relative pixel intensity difference of the background and the areas with different indices of refraction. The intensity of the background determines where the value zero is located within the calibration lens. Knowing the refraction angle allows to calculate the refractive index by using the following two equations:

$$\frac{r}{f} = \tan\varepsilon \approx \varepsilon \qquad [7.1]$$

$$\varepsilon_y = \frac{1}{n}\int \frac{\partial n}{\partial y}\partial z = \frac{Z}{n_\infty}\frac{\partial n}{\partial y} \qquad [7.2]$$

where in equation 7.1 f is the focal length of the lens, r is the radius measured from the earlier mentioned value of zero refraction within the lens and ε is the angle of refraction either in x or y direction, depending on the alignment of the cutoff. [3]. These parameters are also shown in Fig. 7.15. In equation 7.2 ε_y stands for the refraction angle in y direction, n_∞ for the index of refraction of the surrounding air and Z for the extent of the schlieren area. The integral can be simplified if the change of the refractive index is assumed to be constant [3].

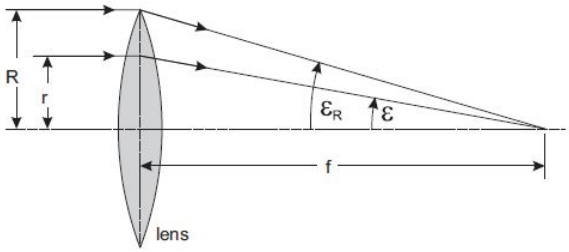

Fig. 7.15: Illustration of the parameters of equation [7.1]. Reproduced from [3] by permission of Dr. M. J. Hargather.

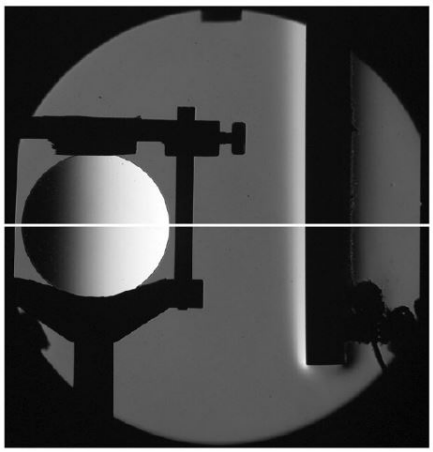

Fig. 7.16: Calibration lens placed next to a heated, flat metal plate. Reproduced from [3] by permission of Dr. M. J. Hargather.

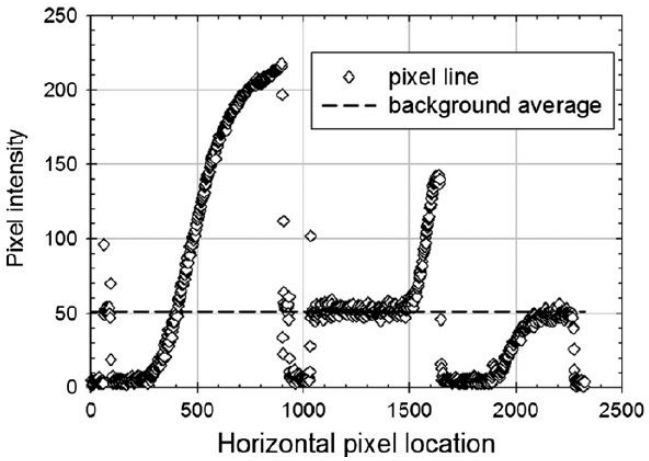

Fig. 7.17: Pixel intensity dependent on the horizontal pixel location with a graded cutoff. Reproduced from [3] by permission of Dr. M. J. Hargather.

Fig. 7.16 shows the experiment implemented by Hargather and Settles [3]. A heated, flat metal plate and a calibration lens were placed within the collimated light beam of a Z-type schlieren system. The horizontal line in Fig. 7.17 is where the taken picture was evaluated. It shows the pixel intensity over the horizontal pixel location, whereas the background intensity is highlighted by a dashed line in Fig. 7.17. The two different cutoffs, the regular cutoff and the graded filter cutoff, were placed in vertical direction. While the regular knife-edge cutoff was able to provide higher sensitivity, the

graded filter had a wider measurement range, as shown in Fig. 7.18 [3].

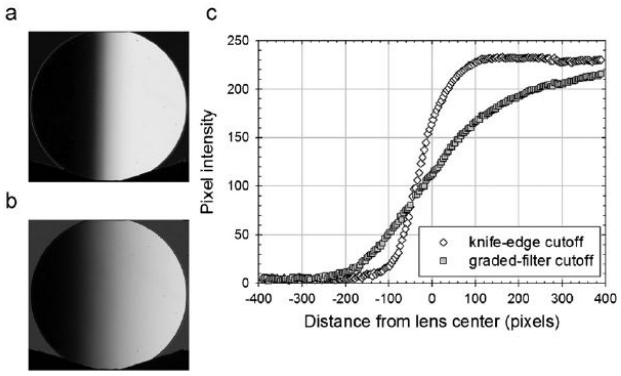

Fig. 7.18: Different measurement ranges of a knife-edge cutoff (a) and a graded-filter cutoff (b). Reproduced from [3] by permission of Dr. M. J. Hargather.

Hargather and Settles concluded, that for the created thermal boundary layer the regular knife-edge cutoff is the better choice since it provides higher sensitivity which is crucial for a quantitative evaluation [3].

The area around an arc is heated rapidly which means the temperature and density have strong gradients. Consequently, the regular knife-edge cutoff is the right choice for this application.

7.1.6 High-Speed Camera

Acquiring quantitative data from schlieren images already causes a considerable effort, but generating a picture up to every $5\mu s$ with a high-speed camera brings up more difficulties. The high-speed camera Photron APX-RS was not available for tests during the research but is the available equipment if a schlieren system is set up.

The arc breakdown event in a circuit breaker takes place in a few milliseconds which is why a photo should be taken at least every $50\mu s$. At $50\mu s$ or 20000 frames per second (fps) the camera in question reaches a resolution of up to 512×256 pixels, according to Fig. 7.20, with a shutter time of up to $2\mu s$ independent of the frame rate, according to the datasheet [30]. Especially for arc filming a short shutter time is desired due to the fast movement of the arc and the high light intensity.

The earlier explained BOS tests were captured with a camera of a smartphone which had 15.9 megapixels in an $4:3$ image format that resulted in a resolustion of 4608×3456 pixels. Of course, a lower resolution means less data and therefore less accurcy for quantitative evaluation. The comparison of 4608×3456 with 512×256 is shown in Fig. 7.19. It should be noted that the resolution is written as $width \times height$.

If a quantitative evaluation is desired, the resolution is too low for recordings over further distances. For this reason, either Background-oriented schlieren with a very small distance between the camera, the electric arc and the background or a dual-lens or dual-mirror system with a relatively small workspace is possible.

Fig. 7.19: Comparison of 4608 × 3456 pixels with 512 × 256 pixels

6.1.4. Frame Rates and Resolutions

Table 1

Max Resolution (pixels)	Frame Rate (FPS)	Resolution (pixels)					
		128× 16	128×32	128×48	128×64	128× 128	128× 256
1024× 1024	50(PAL)	✓	✓	✓	✓	✓	✓
	60	✓	✓	✓	✓	✓	✓
	125	✓	✓	✓	✓	✓	✓
	250	✓	✓	✓	✓	✓	✓
	500	✓	✓	✓	✓	✓	✓
	1000	✓	✓	✓	✓	✓	✓
	1500	✓	✓	✓	✓	✓	✓
	3000	✓	✓	✓	✓	✓	✓
512×1024	5000	✓	✓	✓	✓	✓	✓
1024×512	6000	✓	✓	✓	✓	✓	✓
640×480	9000	✓	✓	✓	✓	✓	✓
512×512	10000	✓	✓	✓	✓	✓	✓
512×384	12000	✓	✓	✓	✓	✓	✓
256×512	15000	✓	✓	✓	✓	✓	✓
512×256	20000	✓	✓	✓	✓	✓	✓
256×256	28000	✓	✓	✓	✓	✓	✓
	30000	✓	✓	✓	✓	✓	✓
512×128	36000	✓	✓	✓	✓	✓	–
256×128	50000	✓	✓	✓	✓	✓	✓
128×128	60000	✓	✓	✓	✓	✓	–
256×64	75000	✓	✓	–	–	–	–
256×32	100000	✓	✓	–	–	–	–
128×48	125000	✓	✓	✓	–	–	–
	150000	✓	✓	✓	–	–	–
128×32	180000	✓	✓	–	–	–	–
128×16	210000	✓	–	–	–	–	–
	250000	✓	–	–	–	–	–

Fig. 7.20: Resolustion table of the Photron APX-RS [30]

8 Summary/Conclusion

A circuit breaker constitutes an essential component of safety in electrical engineering. In order to gain a better understanding of how electric arcs in circuit breakers emerge, propagate and how their motion is influenced by the surrounding gas flow, Schlieren Photography may be applied. Schlieren Photography makes these physical quantities visible and therefore provides the opportunity to calibrate such a system and perform quantitative measurements.

Only Background-oriented Schlieren tests were implemented because dual-lens and dual-mirror systems require specific optical equipment such as an optical bench, mirrors and lenses which can cost a fair amount of money. The equipment for Background-oriented Schlieren tests was available without any additional costs, since nowadays almost every smartphone takes high-resolution photos. At first, the main focus was on how to calibrate such a Background-oriented Schlieren system and how the quantification can be performed. Different background patterns were used as shown in Chapter 7 - Tests and Results.

The first test, which was performed with a projector that projected the pattern onto a wall, delivered results with high quality but not good or consistent enough for quantitative evaluation. The need for fixing not only the camera but also the projector would make the setup more complex. For this reason, calibration or evaluation with this setup was no longer pursued.

For the second test the background pattern was printed and fixed onto a wall. The advantage of this arrangement was less degrees of freedom because the background was not moveable any more. The calculation of the offset vectors with OpenPIV provided viable results which could be pursued to obtain the actual density and temperature if all geometrical parameters are known.

Whether Background-oriented Schlieren, a mirror system or a lens system fulfil the requirements best depends heavily on the accessibility of the electric arc. If there is enough space to place a certain background pattern behind the area the arc is going to occur and necessary precautions are made, Background-oriented Schlieren remains to be the cheapest possible setup. It should be noted that the dots on the background should have at least the size of three or four pixels on the photo to provide best quality [31].

If it is possible for a light beam to pass through the area the arc is going to occur, a lens or mirror based system could be used, too. Both of these setups would, compared to Background-oriented Schlieren, cost a fair amount of money which should be taken into account when choosing a setup. Also, the length of the arrangement that increases with the diameter of the lenses and mirrors may cause a problem. However, the sensitivity to vibrations is by far not as problematic as with Background-oriented Schlieren and the modifications to enable color schlieren if a color camera is available are negligible.

9 Future Work

9.1 Color or Rainbow Schlieren

The Photron APX-RS is a monochrome camera which means that only grayscale photos can be recorded. Due to the fact that the information about density and temperature in schlieren photos is kept within the intensity of the photo, it does not cause any issues, although there are different ways to calibrate and evaluate a schlieren image. One of them is called color schlieren or rainbow schlieren [1].

If the regular knife-edge cutoff in a dual-mirror or -lens system is replaced by a "rainbow" cutoff or more accurat filter, the information about the changes in the index of refraction is no longer stored in the intensity or brightness of the image but in the color and intensity of the resulting image, depending on the cutoff filter. Fig. 9.1 shows different types of color filter.

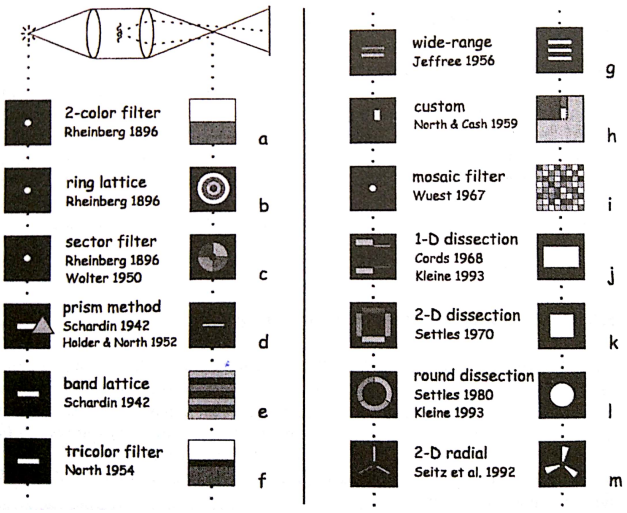

Fig. 9.1: Different color schlieren filter. Reproduced from [1] by permission of Dr. G. S. Settles

How these filters work in detail is explained in [1]. The main difference is that no matter in which direction the light is deflected, it appears on the background. The data of its deflection and therefore the information about the index of refraction is stored in the color. If a color camera is available, the calibration and evaluation could be performed similar to the calibration explained in section 7.1.5.

10 List of Figures

11 Bibliography

[1] G. S. Settles, *Schlieren and Shadowgraph Techniques: Visualizing Phenomena in Transparent Media*. Springer Science & Business Media, 2001. Google-Books-ID: HWtB2R0gWFgC.

[2] F. Klinge, T. Kirmse, and J. Kompenhans, *Application of Quantitative Background Oriented Schlieren (BOS): Investigation of a Wing Tip Vortex in a Transonic Wind Tunnel*. Jan. 2004.

[3] M. J. Hargather and G. S. Settles, "A Comparison of Three Quantitative Schlieren Techniques," *Optics and Lasers in Engineering*, vol. 50, pp. 8–17, Jan. 2012.

[4] R. Smeets, L. v. d. Sluis, M. Kapetanovic, D. F. Peelo, and A. Janssen, *Switching in Electrical Transmission and Distribution Systems*. John Wiley & Sons, Jan. 2015. Google-Books-ID: UwIaBgAAQBAJ.

[5] "Circuit Breaker Characteristic Trip Curves and Coordination."

[6] P. Zeller, "Lecture Electrical Engineering, University of Applied Sciences Upper Austria Campus Wels."

[7] "Physik - für Wissenschaftler und Ingenieure | Paul A. Tipler | Springer."

[8] "https://www.ledgrowlight-hydro.com/ledlights-blog/choosing-the-right-kind-led-grow-lights-is-extremely-important/."

[9] "https://micro.magnet.fsu.edu/primer/java/electromagnetic/index.html."

[10] "https://en.wikipedia.org/w/index.php?title=Refraction&oldid=821729505," Jan. 2018. Page Version ID: 821729505.

[11] J. E. Hartberger, *Background-oriented Schlieren Pattern Optimization*. 2011. Google-Books-ID: OV8kMwEACAAJ.

[12] "https://en.wikipedia.org/w/index.php?title=Cross-correlation&oldid=817992773," Dec. 2017. Page Version ID: 817992773.

[13] "2-D cross-correlation - MATLAB xcorr2 - MathWorks Deutschland - https://de.mathworks.com/help/signal/ref/xcorr2.html."

[14] A. J. I. Toepler and W. Ostwald, *Ostwalds Klassiker der exakten Wissenschaften*. W. Engelmann, 1906. Google-Books-ID: xt4rAQAAMAAJ.

[15] G. S. Settles and M. J. Hargather, "A review of recent developments in schlieren and shadowgraph techniques," *Measurement Science and Technology*, vol. 28, Jan. 2017.

[16] "https://www.labcompare.com/1344-High-Speed-Camera/3677-FASTCAM-APX-RS-High-Speed-Camera/."

[17] "http://www.ozscopes.com.au/fotopro-aluminium-mini-tripod-black.html."

[18] "Amazon.com: Vastar Universal Cell Phone Tripod Mount Adapter Holder for iPhone/Samsung Galaxy/Nexus and More Cell Phones Use on Tripod, Monopod, Selfie Stick, Tabletop Tripod Stand and More: Cell Phones & Accessories."

[19] "http://www.hcinema.de/pro/anzeigen.php?angabe=dell2300mp."

[20] "http://www.fast.u-psud.fr/~moisy/ml/."

[21] Z. J. Taylor, R. Gurka, G. A. Kopp, and A. Liberzon, "Long-Duration Time-Resolved PIV to Study Unsteady Aerodynamics," *IEEE Transactions on Instrumentation and Measurement*, vol. 59, pp. 3262–3269, Dec. 2010.

[22] L. Venkatakrishnan and G. E. A. Meier, "Density measurements using the Background Oriented Schlieren technique," *Experiments in Fluids*, vol. 37, pp. 237–247, Aug. 2004.

[23] G. Guang-Ming, "Density and temperature reconstruction of a flame-induced distorted flow field based on background-oriented schlieren (BOS) technique."

[24] "https://en.wikipedia.org/w/index.php?title=Chromatic_aberration&oldid=812036489," Nov. 2017. Page Version ID: 812036489.

[25] "https://www.dkfindout.com/us/science/light/splitting-light/."

[26] "https://photographylife.com/what-is-spherical-aberration."

[27] "https://www.edmundoptics.com/optics/optical-mirrors/focusing-concave-mirrors/precision-parabolic-mirrors/."

[28] "https://de.wikipedia.org/w/index.php?title=Abbildungsfehler&oldid=169904450," Oct. 2017. Page Version ID: 169904450.

[29] "https://en.wikipedia.org/w/index.php?title=Astigmatism_(optical_systems)&oldid=796395398," Aug. 2017. Page Version ID: 796395398.

[30] "http://www.highspeedimaging.com/media/photron_manuals/FASTCAM-APX_rs_hw_manual.pdf."

[31] M. Raffel, "Background-oriented schlieren (BOS) techniques," *Experiments in Fluids*, vol. 56, p. 60, Mar. 2015.